Journal of Hazardous Materials 381 (2020) 121233

Contents lists available at ScienceDirect

Journal of Hazardous Materials

journal homepage: www.elsevier.com/locate/jhazmat

Facile synthesis of aluminum branched oligo(phenylphosphonate) submicro-particles with enhanced flame retardance and smoke toxicity suppression for epoxy resin composites

Yao Yuan[a,b], Yongqian Shi[c], Bin Yu[d], Jing Zhan[e], Yan Zhang[b], Lei Song[b], Chao Ma[b,*], Yuan Hu[b,*]

[a] Fujian Provincial Key Laboratory of Functional Materials and Applications, School of Materials Science and Engineering, Xiamen University of Technology, Xiamen 361024, PR China
[b] State Key Laboratory of Fire Science, University of Science and Technology of China, Hefei 230026, PR China
[c] College of Environment and Resources, Fuzhou University, Fuzhou 350002, PR China
[d] Centre for Future Materials, University of Southern Queensland, Toowoomba, QLD 4350, Australia
[e] School of Civil Engineering and Environmental Engineering, Anhui Xinhua University, Hefei, Anhui, 230088, PR China

GRAPHICAL ABSTRACT

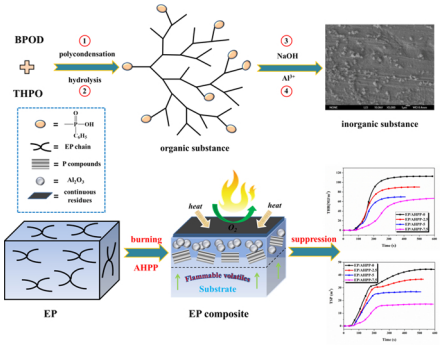

ARTICLE INFO

Editor: Daniel CW Tsang

Keywords:
Epoxy resins
Branched flame retardant
Submicro-scale particles
Smoke toxicity suppression

ABSTRACT

A novel and submicro-scale aluminum branched oligo(phenylphosphonate) (AHPP) has been successfully synthesized and embedded into a polymeric substrate to improve the fire safety of epoxy resin (EP). The chemical structures of intermediates and target products were characterized using the nuclear magnetic resonance spectroscopy, X-ray diffraction and Fourier transform infrared analysis. Morphology analysis confirmed that all of the as-synthesized AHPP submicro-particles are mutually well-separated. Combustion results demonstrated that the limiting oxygen index value is increased to 30.5% from 23.5% while the PHRR and THR are decreased by ca. 68.1% and 41.2%, respectively for the EP/AHPP-7.5 composite compared to the corresponding values for pure EP. In addition, the binary blends display the satisfying smoke toxicity suppression performance during combustion. The total smoke production and the total CO yield for EP/AHPP-7.5 are dramatically reduced by 62.0% and 32.3%, respectively, which may mainly be ascribed to the catalytic carbonization performance of the polymers and formation of Al_2O_3 layers on the surface of the char residues. As a result, the findings in this study enabled the submicro-scale phosphorus-containing flame retardant to be a potential candidate as an efficient additive for reducing smoke toxicity of polymer composites.

* Corresponding authors.
E-mail addresses: mcsky@ustc.edu.cn (C. Ma), yuanhu@ustc.edu.cn (Y. Hu).

https://doi.org/10.1016/j.jhazmat.2019.121233
Received 6 March 2019; Received in revised form 4 September 2019; Accepted 13 September 2019
Available online 14 September 2019

1. Introduction

Epoxy resin is a significant member of a class of thermosetting polymers. These materials are endowed with outstanding properties and great versatility and are widely applied in the areas of encapsulation, laminate formation, coatings, adhesives and insulating materials (Auvergne et al., 2013; Gu et al., 2016). Nonetheless, EPs exhibit high flammability, a major limitation, which greatly restricts applications in many areas such as transportation, construction, aerospace and electronics (You et al., 2015; Wan et al., 2012; Jian et al., 2016; Wan et al., 2015). Moreover, the formation of toxic gases and visible smoke during combustion present challenges to people escaping from fires and lead to mass casualties and property damage. Herein, a considerable number of research efforts of reducing the fire hazard for EP are vital to human society.

Multiple methods have been utilized for reducing the flammability of epoxy resin. These include incorporating of various flame retardant species such as phosphorus- (Shi et al., 2018), nitrogen- (Xu et al., 2018), silicon- (Mercado et al., 2006; Zhou et al., 2018) and boron-containing (Dogan and Unlu, 2014; Yu et al., 2016) compounds into the resin. Over the years, phosphorus-containing flame retardants have attracted increasing attention. Some of these can improve flame retardance by action both in gaseous and condensed phases (Zang et al., 2011; Ma et al., 2017). Among these compounds (Ren et al., 2007; Chen et al., 2010; Jeng et al., 2002; Kandola et al., 2010), the simultaneous incorporation of various phosphorus-containing groups is a very effective way to impart good flame resistant properties (Zhang et al., 2017). Braun et al. (2006) presented a comparative study of the impact of the presence of phosphorus-containing species in epoxy resin has been presented. A mode of action for these compounds based on the thermal decomposition behavior of two EPs was proposed. The flame retardants differed in the nature of bonding to phosphorus atoms. Both P—C and P—O—C bonds were present and the prominence of condensed-phase or gas-phase activity depends somewhat on the reactions and interactions between the EP substrate and the flame retardants. However, it largely determined by the level of oxygenation at phosphorus. Phosphates are generally active in the condensed-phase while phosphonate and phosphinates are often active in the gas-phase (Howell et al., 2018).

Branched polymers with a high density of active terminal groups and imperfect tree-like structure, in comparison with linear counterpart with similar molecular weight (Huang et al., 2009; Liu et al., 2009), have received extensive attention due to the extraordinary architecture and unique physicochemical performance (Wang et al., 2006a; Täuber et al., 2014). It is notable that widespread applications of branched polymers have been found in diverse fields, such as flame retardance (Chen et al., 2011; Wang and Shi, 2006a; Feng et al., 2018a; Li et al., 2014), resin tougher (Choi and Kwak, 2007) and plasticizer (Boogh et al., 1999) due to low vilscosity and melting point (Pinto et al., 2001). Herein, it is of great interest to modify novel branched phosphorus-containing additives are attractive because of simple preparation and easy-to-tailor structures of branched polymers.

To overcome the intrinsic high flammability and smoke toxicity of EPs during combustion, it is proposed to design novel and submicro-scale aluminium branched oligo(phenylphosphonate) (AHPP) has been prepared with different oxidation states (-1, +3) via polycondensation. This report presents impressive results regarding the enhancement of flame retardance and smoke toxicity suppression performance for EP/AHPP blends. Fourier transform infrared spectroscopy (FTIR), X-ray diffractometry (XRD), nuclear magnetic resonance spectroscopy (^{1}H and ^{31}P NMR), scanning electron microscopy (SEM), and transmission electron microscopy (TEM) were applied to verify the chemical structure and morphology of obtained samples. Furthermore, a mode of reduction of fire hazards for the EP/AHPP system has been proposed. The findings reported suggest that submicro-scale phosphorus-containing flame retardant to be a potential candidate as a new efficient agent with enhanced fire hazards suppression performance for polymeric materials.

2. Experimental section

2.1. Materials

Benzene phosphorous oxydichloride (BPOD) was purchased from Sun Chemical Technology Co., Ltd., Shanghai, China. Tetrakis(hydroxymethyl)phosphonium sulfate (THPS, 75% aqueous solution) was obtained from Aladdin Chemistry Co. Ltd., China. DGEBA type epoxy resin was provided by Jiangfeng Chemical Industry Co. Ltd. (Anhui, China). Barium hydroxide ($Ba(OH)_2.8H_2O$), hydrogen peroxide, 4,4′-diaminodiphenylmethane (DDM), aluminum sulphate ($Al_2(SO_4)_3{\cdot}18H_2O$), ethyl acetate, anhydrous sodium sulfate and sodium chloride were all supplied by Sinopharm Chemical Reagent Co. Ltd. (Shanghai, China).

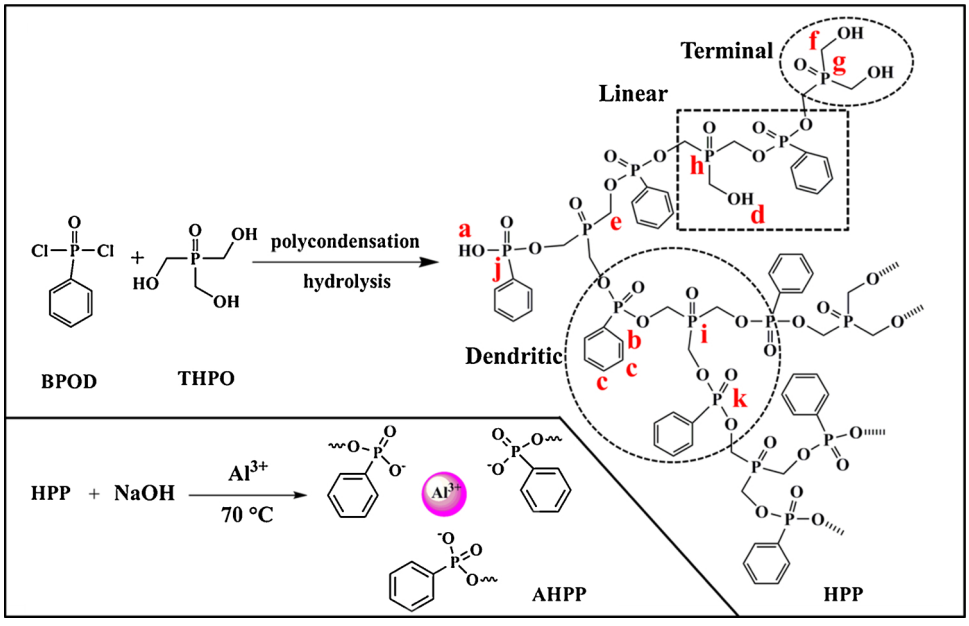

Scheme 1. Synthetic Route for AHPP via the polycondensation of THPO with BPOD.

2.2. Synthesis of THPO

$Ba(OH)_2.8H_2O$ (0.35 mol) was firstly dissolved in 300 mL of distilled water at 70 °C and then added into 75% THPS (0.35 mol) aqueous solution. Subsequently, the reaction was kept at 25 °C for 2 h with continuous agitation. After the white precipitate was separated by centrifugation, hydroperoxide aqueous solution (0.7 mol) was dropwise added to the supernatant at 0 °C for 3 h, followed by removing water under reduced pressure. Herein, the high-yield final product THPO (a colorless liquid) was obtained.

2.3. Synthesis of the intermediate product

The synthetic route of the branched oligo(phenylphosphonate) precursor was displayed in Scheme 1. Typically, a three necked round-bottomed flask was flushed with 0.3 mol of BPOD, which was equipped with reflux condenser, nitrogen inlet and mechanical stirrer, followed by slowly adding THPO (0.15 mol). The reaction kept going at 100 °C for 5 h under mechanical stirring in an inert atmosphere. The reaction temperature was then declined to 70 °C with 60 mL of deionized water, and the mixtures were further agitated for 1.5 h. After hydrolyzation of the precursor and removing of the water, Ethyl acetate was added to dissolve, and the solution was then washed three times with a saturated sodium chloride. After that, the mixture was dried and evaporated to dryness to obtain a white solid which was collected for testing.

2.4. Synthesis of submicro-scale target product

The above intermediate was dissolved in 50 mL of deionized water with mechanical stirring in a three necked reaction vessel. The acidic solution was adjusted to neutral with sodium hydroxide. After the mixture was heated to 65 °C, a solution of $Al_2(SO_4)_3{\cdot}18H_2O$ (0.05 mol) in 25 mL of H_2O was added dropwise and the resulting mixture was kept for 2 h. After cooling to 25 °C, the target product was collected by filtration at reduced pressure and washed repeatedly till the PH value of the filtrate was 7. The obtained white powder was dried at 90 °C for 20 h and the yield was > 90.0%.

2.5. Preparation of flame-retardant EP and the control sample

Submicro-scale aluminium branched oligo(phenylphosphonate) (AHPP) was firstly dispersed in DGEBA uniformly with constant agitation at 100 °C for 1.5 h, followed by the dispersion into acetone. After removing the solvent for 2 h, the DDM was added. Subsequently, the mixture was quickly poured into a preheated mould, curing at 100 °C for 2.5 h and postcuring at 150 °C for another 2.5 h. The final samples with 0, 2.5, 5 and 7.5 wt % AHPP were labeled as EP/AHPP-0, EP/AHPP-2.5, EP/AHPP-5 and EP/AHPP-7.5.

2.6. Characterization

Nuclear magnetic resonance (NMR) spectroscopy was conducted using an AVANCE 400 Bruker spectrometer with DMSO-d_6 and D_2O as the solvent.

Fourier transform infrared spectroscopy was recorded on a Nicolet 6700 spectrometer (Nicolet Instrument Company, USA) with KBr pellets.

The crystal-phase property of the EP composite was studied by a powder X-ray diffractometer (Japan Rigaku D Max-Ra) using a rotating anode X-ray diffractometer accompanied with a Ni filtered Cu-Ka tube ($\lambda = 1.54178$ Å) in the 2θ range from 10° to 70° with a sweep speed of 4 min^{-1}.

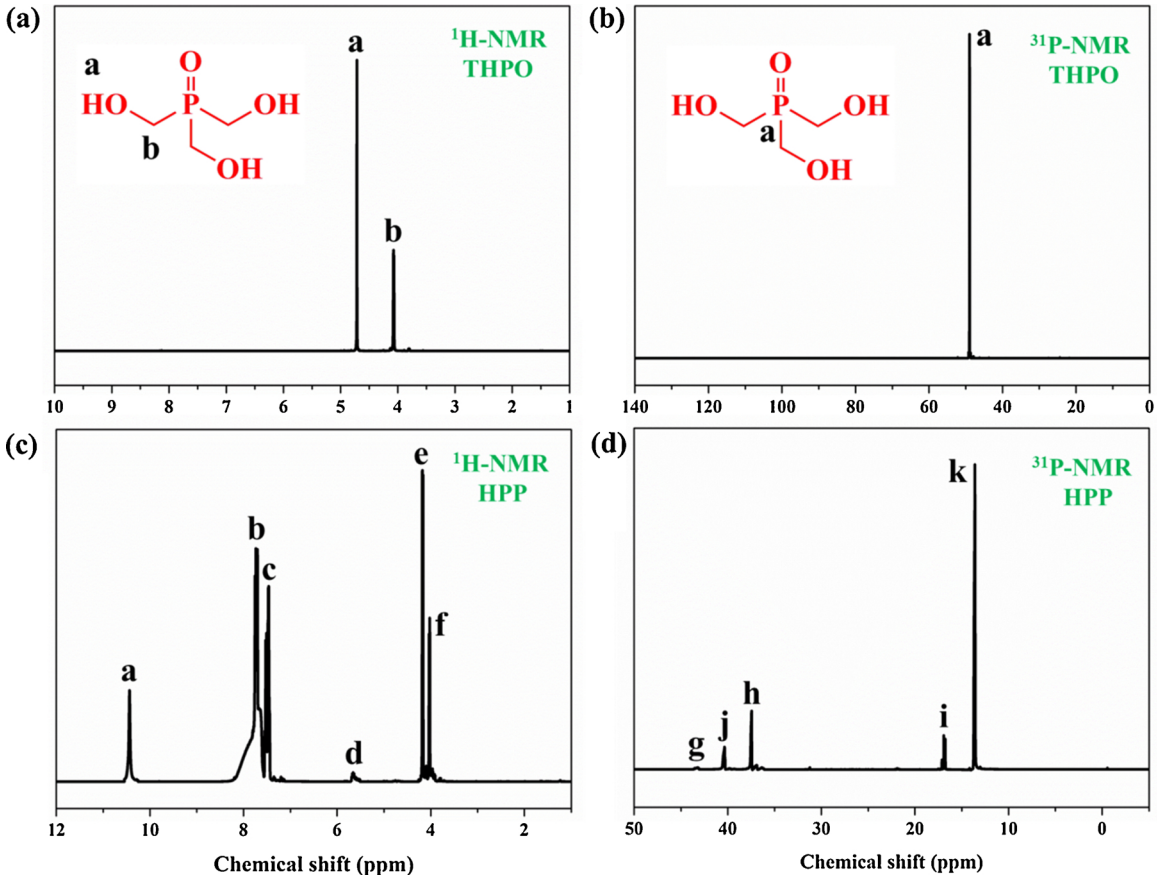

Fig. 1. The ^1H NMR spectrum (a) and ^{31}P NMR spectrum (b) of THPO with D_2O as the solvent, the ^1H NMR spectrum (c) and ^{31}P NMR spectrum (d) of HPP with DMSO-d6 as the solvent.

The element composition and morphology of submicro-scale AHPP were investigated by a KYKY1010B scanning electron microscope (SEM) and a JEOL2010 transmission electron microscopy with an accelerating voltage of 200 kV. Prior to observation, the samples were dispersed in ethanol with adequate ultrasound and then dropped on copper grids.

Gel permeation chromatography (GPC) was measured with an instrument equipped with a G1310B ISO pump, a G1316A PLgel column, and a G1362A differential refractive index detector.

Combustion properties of EP and its composites were performed on a microscale combustion calorimeter (MCC, GOVMARK) and thermal stability was analyzed with thermogravimetric analysis (TGA) using a Q5000IR thermo-analyzer instrument with approximate 3.6 mg samples at a linear heating rate of 20 °C/min from room temperature to 800 °C.

The thermo-oxidative degradation of EP composite was determined by Real-time Fourier transform infrared spectroscopy, which was performed in the range of room temperature to 600 °C at a heating rate of around 10 °C/min under air on a MAGNAIR 750 spectrometer equipped with a heating device and a temperature controller.

Limiting oxygen index (LOI) test was conducted using a HC-2 oxygen index meter according to ASTM D2863. Size of the specimen for the measurement was 100 × 6.5 × 3.0 mm^3.

The vertical burning (UL-94) test was performed on a CFZ-II horizontal and vertical burning tester with a sample dimension of 127 × 12.7 × 3 mm^3 on the basis of ASTM D3801.

Cone calorimeter (Stanton Redcroft, UK) test was conducted according to ISO 5660 standard. Each specimen was wrapped with aluminum foil and burned at an external heat flux of 35 kW/m^2 with the size of 100 × 100 × 3 mm^3.

The smoke toxicity test was assessed and performed according to ISO TS 19,700 using a steady state tube furnace tests (SSTF). 20 g of samples in the form of granules, which were spread evenly along the combustion quartz boat in the tube furnace with 825 °C at a constant air flow rate.

The quantitative measurement of the evolved gases was conducted by the tubular furnace method. 0.5 g of samples loaded into the crucible are fed into the furnace with 800 °C for at least 18 min. The combustion gases were continuously extracted using a pump with 2 L min^{-1}.

Thermogravimetric analysis/infrared spectrometry (TG-IR) of EP and EP composites was carried out through a TGA Q5000 thermogravimetric analyzer using approximate 3 mg samples, which used a stainless steel transfer pipe to combine with a Nicolet 6700 spectrophotometer. Thermal analyzer was conducted in the range from 25 °C to 700 °C with a heating rate of 20 °C/min under a nitrogen condition.

The char residue of EP composite after cone calorimeter test was observed by a KYKY1010B scanning electron microscope. The sample was coated with gold/palladium alloy.

Raman spectra of the char after cone calorimeter tests were recorded on a SPEX-1403 laser Raman spectrometer (SPEX Co., USA).

3. Results and discussion

3.1. Structural characterization and morphology

Fig. 1 presents (a) ^1H NMR and (b) ^{31}P NMR spectra of THPO. The peak at 4.72 ppm is characteristic of O═P−CH_2−O, and the single peak at 4.08 ppm corresponds to hydroxyl proton (C−OH) in the ^1H NMR spectrum. Fig. 1b displays only one sharp signal for phosphorus which appears at 49.95 ppm.

Fig. 1c and d show ^1H and ^{31}P NMR spectra of HPP, the signals between 7.39–8.30 ppm is ascribed to the hydrogen on aromatic ring. The peak at 10.45 ppm corresponds to proton of O═P−OH and the chemical shift at 5.5 ppm is characteristic of hydroxyl proton on P−⊖CH_2−OH. The signal at 4.06 ppm is contributed to the methylene proton of O═P − CH_2−OH. Moreover, signals between 4.10 and 4.24 ppm is caused by the methylene proton of Ph−P(═O)−O−⊖CH_2−P═O, which verifies the reaction between THPO and BPOD.

The structure and molecular weight of HPP is determined by ^1H NMR, ^{31}P NMR spectrums and GPC. The molecular weight of AHPP was acquired from GPC, and the number-average molecular weight is 2100 g/mol with the polydispersity index of 1.3. In a branched polymer, The peaks situated at 43.2, 37.4, and 16.8 ppm are due to the O═P(−CH_2−)$_3$ with one, two, and three hydroxyls reacted, respectively, which are identified as terminal (T), dendritic (D) and linear (L) units (Xie et al., 2008). As shown in Fig. 1d, peak i, h and g are corresponding to D, L and T units, respectively. The ratio between linear and branching units refers to the ratio of integral area of peak h to i is 4.3. The structural perfection of a branched polymer can be analyzed by DB, and the following equation was presented:

$$DB = \frac{2D}{2D + L}$$

The DB value can be estimated by the integral intensity of peak i and h in ^{31}P NMR spectrum of HPP to be 0.32. Therefore, the oligomeric structure of HPP is verified.

The FT-IR spectrum (Fig. 2a) was used to further confirm the structure of target product AHPP. It is noticeable that the presence of absorption peaks due to multiple functional groups, such as O−H (3414 cm^{-1}), C–H (2923, 2853 cm^{-1}), P−CH_2 (692, 746 cm^{-1}), P-Ph (1440 cm^{-1}) (Daasch and Smith, 1951). The peak at 1150 cm^{-1} corresponds to the O═P−C and P═O stretching vibrations (Yuan et al., 2016). Moreover, the absorption at 1080 cm^{-1} (Wang and Shi, 2006b), which is caused by the P−O−C bond in AHPP, verifies the successful linkage between THPO and BPOD. The XRD pattern for aluminum branched oligo(phenylphosphonate) (AHPP) submicro-particle is shown in Fig. 2b, the final product of AHPP exhibits major sharp peaks at 2θ = 31.8°, 45.6°, 56.7° and 66.2°, suggesting the creation of a crystal structure.

The morphologies of the AHPP submicro-particles are presented in Fig. 3 by SEM and TEM measurements. It is noted that the as-synthesized AHPP displays submicro-scale and uniform particles. Generally,

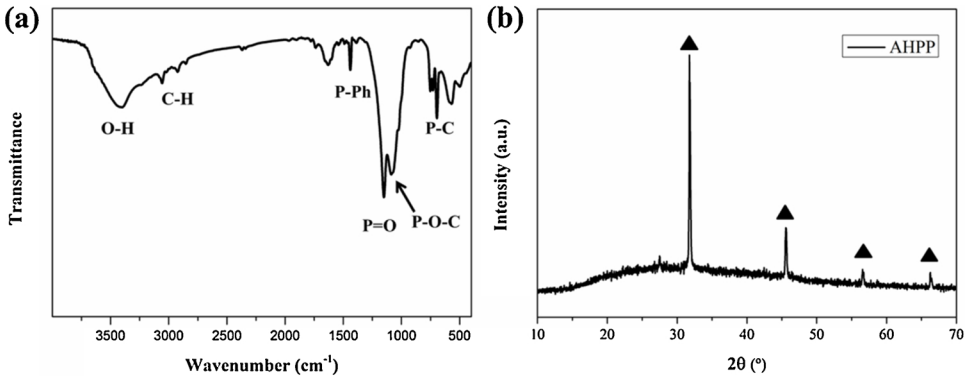

Fig. 2. FTIR spectrum and XRD pattern of AHPP.

reducing the particle size and increasing the morphological homogeneity of the powders plays an increasingly important role in synthesis and processing. Meanwhile, all of the particles are mutually well-separated, producing well-dispersed and homogeneous AHPP submicro-particles. Additionally, EDX was applied to reveal the surface element information in the AHPP submicro-particles. The signals of P, O and Al can be discovered in the EDX spectrum (Fig. 3d), further indicating the successful generation of AHPP submicro-particles.

3.2. Thermal properties of EP and EP/AHPP composites

The influence of AHPP on thermal behavior of cured EP was analyzed by TGA under different atmospheres. TGA and DTG curves of EP and EP/AHPP samples are depicted in Fig. 4. In addition, Table 1 lists sample descriptions, T_d, T_{max}, as well as the flame retardant content and char yield at 800 °C of the final materials. It is noticeable that the EP displays single-step thermal decomposition process under nitrogen (Fig. 4a), and a two-stage steps in air condition (Fig. 4b) refer to the DTG profile (Camino et al., 1984). As seen in Fig. 4a, the AHPP has lower initial decomposition temperature in contrast to EP (378 °C). The reduced T_d value (364 °C) of EP/AHPP-7.5 composite is mainly due to the point that the weak P—O—C and O═P—O bonds in AHPP (Wang et al., 2011; Xu et al., 2015). Nevertheless, increasing the AHPP content can enhances the volume of char residues at 800 °C, and 21.6 wt% is obtained for EP/AHPP-7.5 while EP only lefts residue of 11.2 wt%. To investigate the enhancement of submicro-scale AHPP particles on the thermal resistance of the EP composites, it is assumed that the Y^{cal} of EP/AHPP-7.5 follow the linear mixing rule, as shown in Eq. (1) (Shi et al., 2019).

$$Y^{cal} = Y_{EP} \times f_{w,EP} + Y_{AHPP} \times f_{w,AHPP} \quad (1)$$

Where Y_{EP}, Y_{AHPP}, $f_{w,EP}$ and $f_{w,AHPP}$ represent the residual yield and the weight fraction of EP and AHPP. The large deviation between the experimental and calculated value indicates that the incorporation of AHPP could enhance the thermal stability of the EP composites. Moreover, the lowest maximum mass loss rate is possessed for EP/AHPP-7.5, suggesting that EP/AHPP functions as an effective barrier to restrain the mass loss during the thermal decomposition (Wu et al., 2009; Shieh and Wang, 2001).

3.3. Flame retardance analysis of cured epoxy resin and EP/AHPP composites

3.3.1. LOI and UL-94

The influence of AHPP on the flame retardance of EP and EP/AHPP was characterized by LOI and UL-94. Compared with the data from Table 2, EP is flammable with a low LOI value of 23.5% and has no UL-94 rating. Nevertheless, the LOI value rises gradually from 23.5% to 30.5% with increasing AHPP content from 0 to 7.5 wt%. The inset of Fig. 5 shows the digital images of EP and EP/AHPP-7.5, revealing that the intumescent char residues from EP/AHPP-7.5 hinder heat transfer and protect the matrix from decomposition. Moreover, the EP/AHPP-7.5 composite reaches V-0 rating, which suggested that the introduction of AHPP can reduce the inflammability of the EP.

3.3.2. Microscale combustion calorimeter

MCC is a dependable measurement to evaluate EP and its composites for the flame retardant performance, and excludes physical factors unrelated to combustion test results, such as swelling, dripping, and masking. Heat release rate (HRR) curves of EP, EP/AHPP-2.5, EP/AHPP-5 and EP/AHPP-7.5 samples are depicted in Fig. 5, It is worth noting that a decrease of 41.9% in the peak heat release rate (PHRR) for EP/AHPP-7.5 composite is achieved compared to EP, while the corresponding value of EP/AHPP-2.5 composite is a little lower. It could be

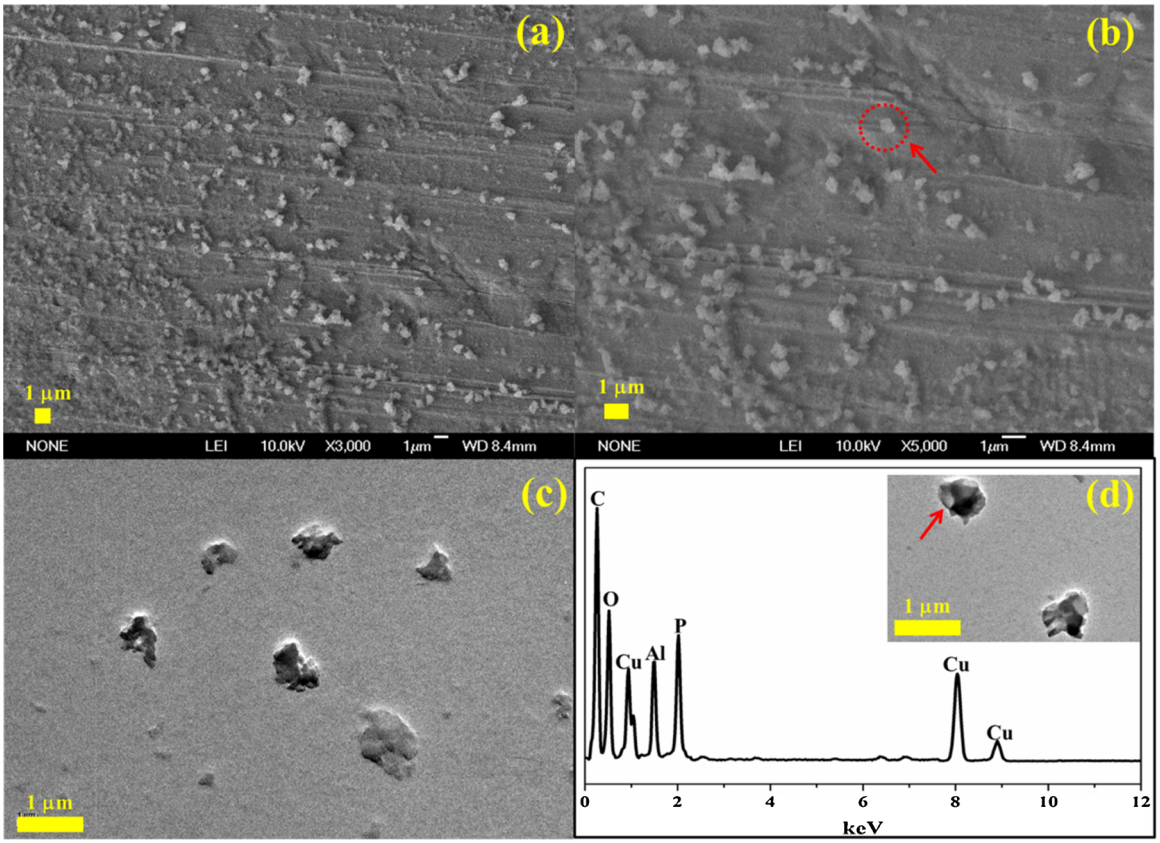

Fig. 3. SEM observations of submicro-scale AHPP: low-magnification (a) and magnified image (b); TEM image of submicro-scale AHPP (c); EDX spectrum of submicro-scale AHPP (d), and the inset is the corresponding TEM image.

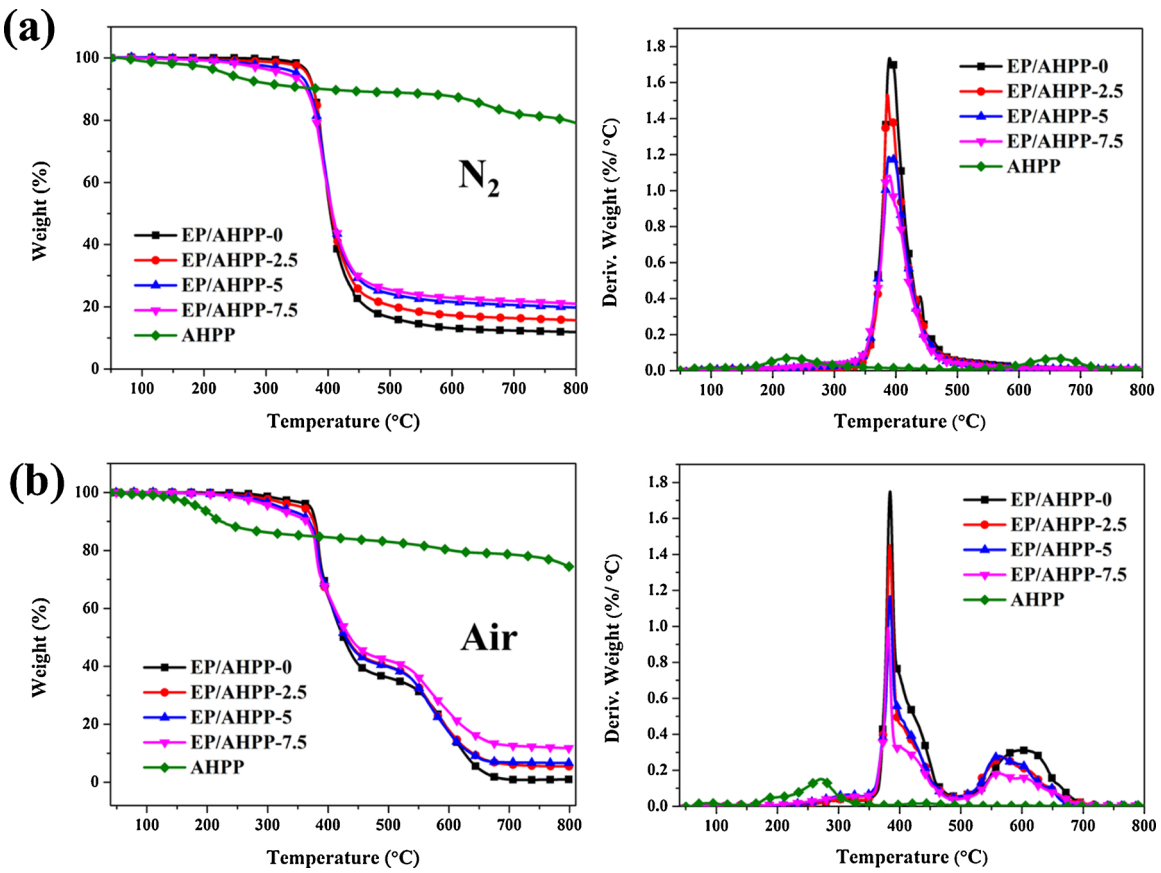

Fig. 4. TGA and DTG curves of AHPP, EP and EP/AHPP composites under nitrogen (a) and air (b).

Table 1
Thermal decomposition data for AHPP, EP and EP/AHPP composites.

Samples	Air				Nitrogen		
	T_d	T_{max1}	T_{max2}	Char (%)	T_d	T_{max}	Char (%)
AHPP	185	273	273	73.7	237	232	79.1
EP	372	384	604	0.85	367	391	11.8
EP/AHPP-2.5	371	385	573	5.5	365	388	15.6
EP/AHPP-5	366	384	563	6.8	350	390	19.7
EP/AHPP-7.5	364	381	564	11.9	331	387	21.1

explained that MCC is based on anaerobe pyrolysis and the needed sample tested by MCC contained only a few milligrams weight (Wang et al., 2011).

3.3.3. Cone calorimeter

To evaluated the combustion behaviors of EP composites, HRR and THR curves of EP and EP/AHPP samples are plotted in Fig. 6, and the relevant cone calorimeter data are recorded in Table 2. It is found that the average EHC (av-EHC) values of EP/AHPP composites decreased

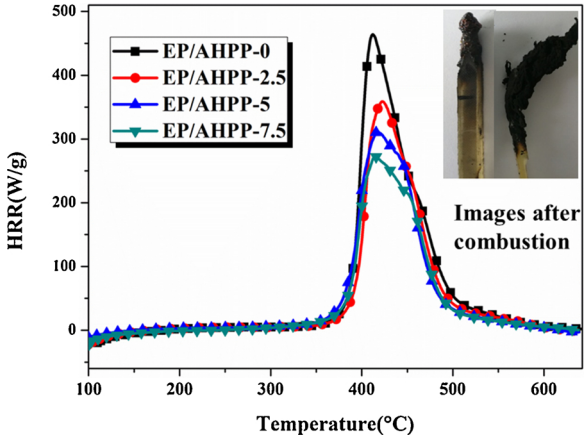

Fig. 5. The heat release rate versus temperature curves of EP and EP/AHPP composites using the microscale combustion calorimeter. Inset: images of EP and EP/AHPP-7.5 after combustion (from left to right corresponding to EP and EP/AHPP-7.5).

Table 2
LOI and UL-94 Rating and cone calorimeter data of EP and EP/AHPP composites.

Samples	LOI (%)	UL-94	TTI (s)	PHRR (kW/m^2)	THR (MJ/m^2)	TSP (m^2)	Av-EHC (MJ/kg)	CY (%)
EP	23.5 ± 0.5	NR	49 ± 2	1425 ± 4	112.9 ± 1.2	44.5	28.36 ± 0.4	10.2
EP/AHPP-2.5	26.5 ± 0.5	NR	66 ± 2	907 ± 5	89.6 ± 1.0	36.8	29.94 ± 0.2	19.3
EP/AHPP-5	28 ± 0.5	V-1	67 ± 3	744 ± 3	69.1 ± 0.6	27.1	32.47 ± 0.3	22.5
EP/AHPP-7.5	30 ± 0.5	V-0	73 ± 2	454 ± 4	66.4 ± 0.8	16.9	34.18 ± 0.1	24.3

partly, which indicates a condensed phase effect (Feng et al., 2012). Moreover, it is noticeable that EP burns rapidly and thus reaches the first main peak at 160 s, presenting a sharp PHRR (1425 kW/m^2). When 2.5 wt % AHPP is added, the PHRR value decreases significantly to 907 kW/m^2. Moreover, the PHRR value of EP/AHPP composite is reduced rapidly when the AHPP content increases. Nevertheless, as shown in Fig. 6a, the faster decomposition of AHPP, the earlier EP substrate to decompose, this is consistent with TGA results in different conditions (Horrocks and Davies, 2000), revealing a formation of protective char and a dramatically enhanced fire retardance of cured epoxy resins.

The curves of THR versus time (Fig. 6b) display that EP burns very fast and fierce, with a maximum value of 112.9 MJ/m^2 reached upon ignition. Meanwhile, the addition of AHPP can prevent the heat release rate gradually with the increment of the AHPP content. For instance, the THR value of EP/AHPP-2.5 sample was reduced to 89.6 MJ/m^2, approximately 20.6% decrease in comparison with EP. The decrease in the THR illuminates that more EP moieties participate into the carbonization process (Wang et al., 2017). All these results clarify that AHPP can availably suppress the combustion and significantly improve the flame resistance of EP composites.

3.4. Smoke toxicity analysis of cured epoxy resin and its composites

Epoxy resins, being inflammable polymers with plenty of organic chains, are easily combustible and generate larger numbers of smoke particles and toxic gases (especially CO) (Feng et al., 2018b), which would dramatically enhance the death rate in fire disaster. Therefore, to meet the requirement of saving lives in the fire, the intensity of attention with efficient flame retardant additive should be drawn to increase. As a fairly useful instrument, the cone calorimeter gives other combustion parameters' values of EP and its composites, such as smoke production rate (SPR) and total smoke production (TSP). Fig. 7c and d provide the smoke evolution information of epoxy composites filled with submicro-scale AHPP particles. It is worthy to note that the smoke particles escaping from combustion of EP composites are distinctly suppressed after introducing 7.5 wt % AHPP submicro-particles (62% reduction for TSP, Fig. 6d). The above-mentioned facts illustrates that the synthesized AHPP submicro-particles endows the epoxy resin with simultaneous higher flame retardance and lower smoke evolution.

The N-Gas model, one of the standards calculating a measure for the toxicity, has been used for toxicity study. To investigate the smoke toxicity suppression behavior of submicro-scale AHPP particles for epoxy resin composites, the amounts of toxic gases were gathered and measured. According to the present work (Yuan et al., 2019), the fire safety of polymer will reduce when the N-Gas value increases (Liu et al., 2016a). Furthermore, the evolution of principal toxicants and the results are presented in Table 3, which indicate that the addition of AHPP particles for reducing the fire hazards is enhanced.

To further investigate the effect of the submicro-scale AHPP particles on the smoke toxicity suppression of epoxy resins, the SSTF test, as a dependable and internationally apparatus for measurement of the smoke toxicity, was recorded in EP and EP/AHPP composites. In the following research, SSTF was applied to inspect CO_2, CO products and smoke density originated from the EP and EP/AHPP composites. As depicted in Fig. 7, the significant decrement in CO, CO_2 and smoke evolution is obtained by the introduction of AHPP submicro-particles, owing to the catalytic carbonization effect of AHPP in EP matrix. These results demonstrate that the earlier degradation of AHPP can catalyze and accelerate the char formation of EP and improve quality and quantity of char layers, which effectually inhibit the mass and heat exchange (Feng et al., 2015; Wang et al., 2013; Li et al., 2017).

TG-FTIR analysis was employed to study the gaseous product in thermal degradation of cured epoxy resin and its composites and further

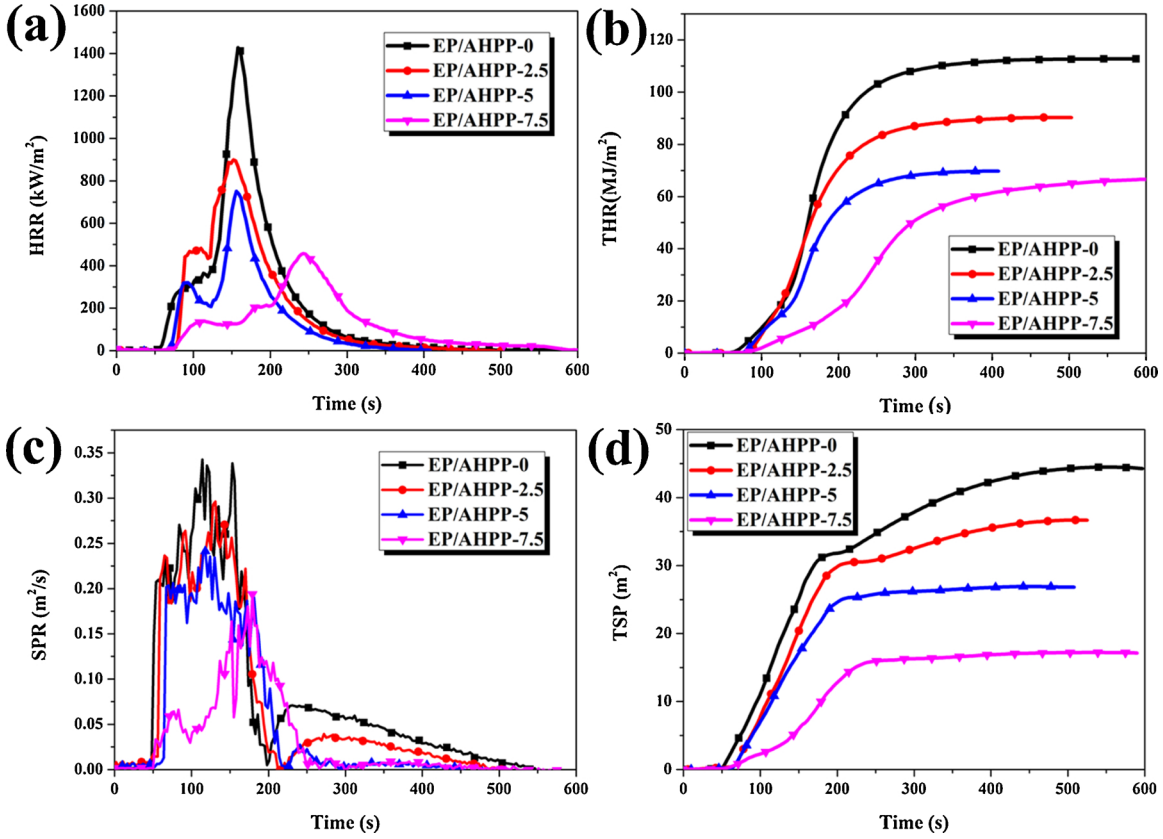

Fig. 6. The heat release rate (a), total heat release (b), SPR (c) and TSP (d) versus time curves of EP and EP/AHPP composites using the cone calorimeter.

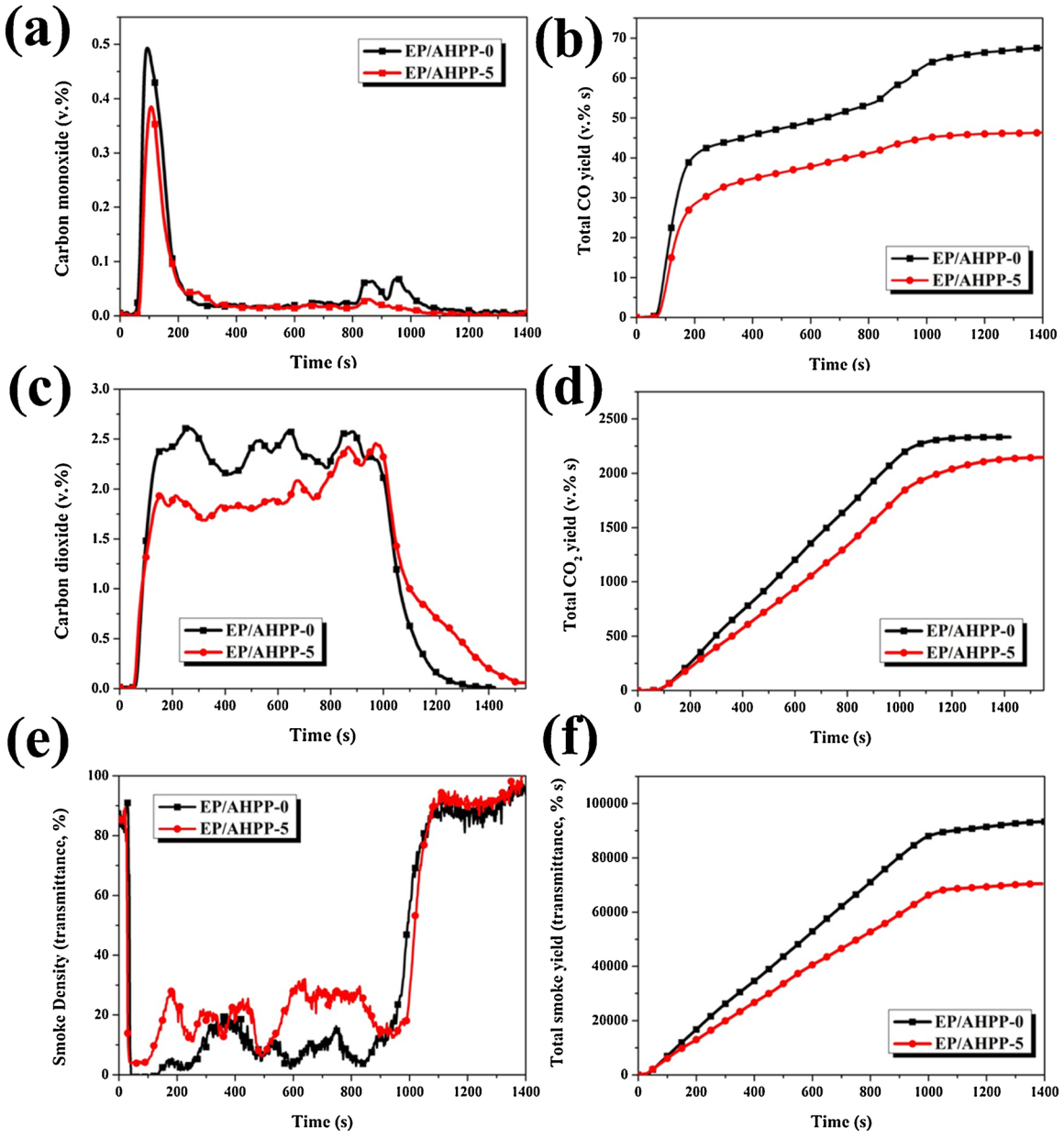

Fig. 7. CO curves (a, b), CO_2 curves (c, d), and total smoke density (e, f) of EP and EP/AHPP-7.5 composite obtained from SSTF tests.

Table 3
Quantitative analysis of gaseous products of degradation of EP and EP/AHPP-7.5 composite by tubular furnace method at 825 °C.

Samples	Products					N-Gas value Eqn.(2)
	HCN (ppm)	NO_x (ppm)	CO (ppm)	CO_2 (ppm)	O_2 (ppm)	
EP	286	135	9000	105000	19.6	2.31
EP/AHPP-7.5	257	112	7200	100000	19.4	1.89

explore the thermal degradation mechanism. The FT-IR analysis at the maximum decomposition rates in a single-stage and the evolution of total gaseous products are displayed from Fig. 8. The decomposition products are distinguished by characteristic FT-IR intensity signals: hydroxide groups (3650–3400 cm^{-1}), hydrocarbons (C—H structure at 2930 cm^{-1}), unsaturated C—H stretching (3108 cm^{-1}) and compounds containing aromatic ring (1605-1450 cm^{-1}, 1260–927 cm^{-1}). It is evident that the typical degradation compounds of different samples are similar whereas

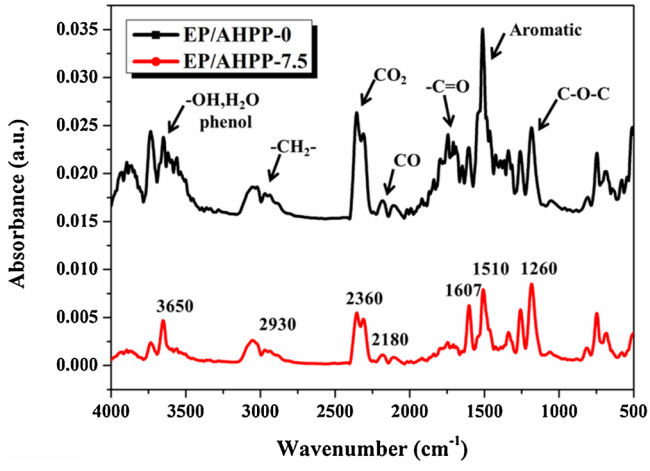

Fig. 8. FT-IR spectrum of pyrolysis products at the maximum decomposition rate of EP and EP/AHPP-7.5 composite.

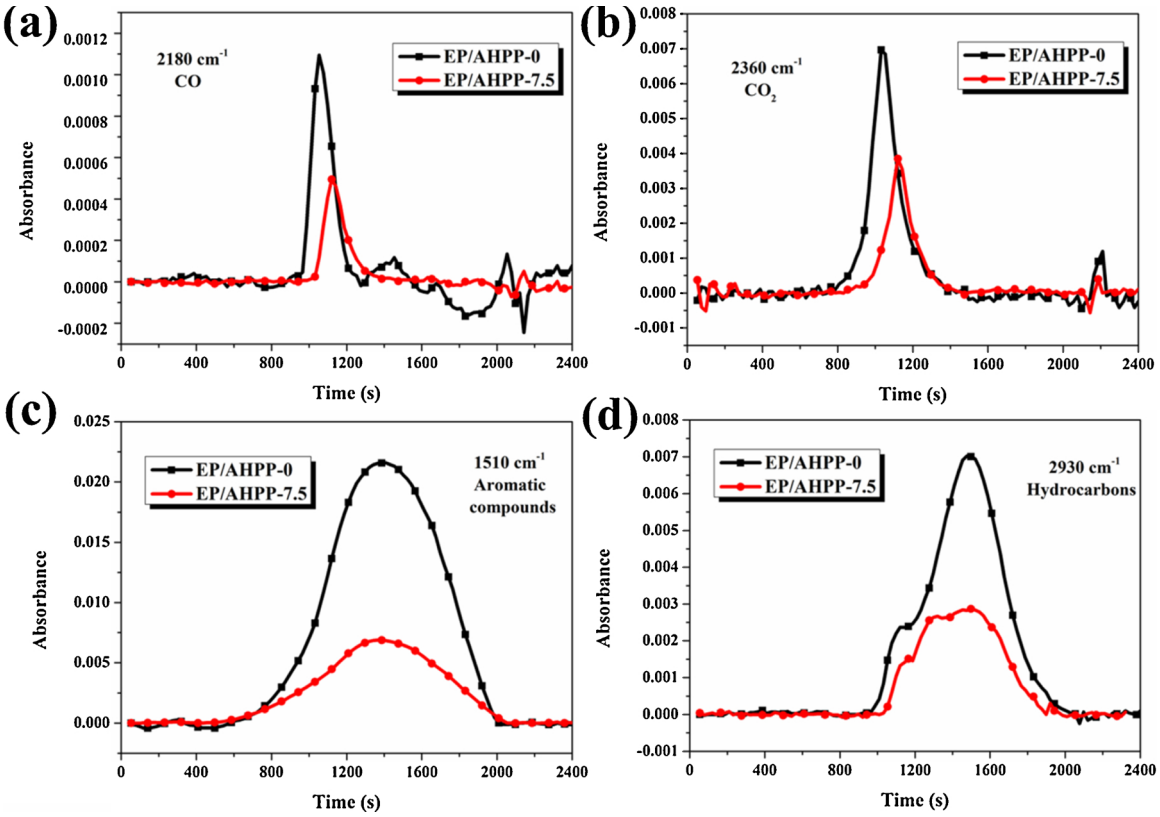

Fig. 9. Absorbance of pyrolysis products in nitrogen atmosphere for EP and EP/AHPP-7.5 composite versus time: CO (a), CO_2 (b), hydrocarbons (c) and aromatic compounds (d).

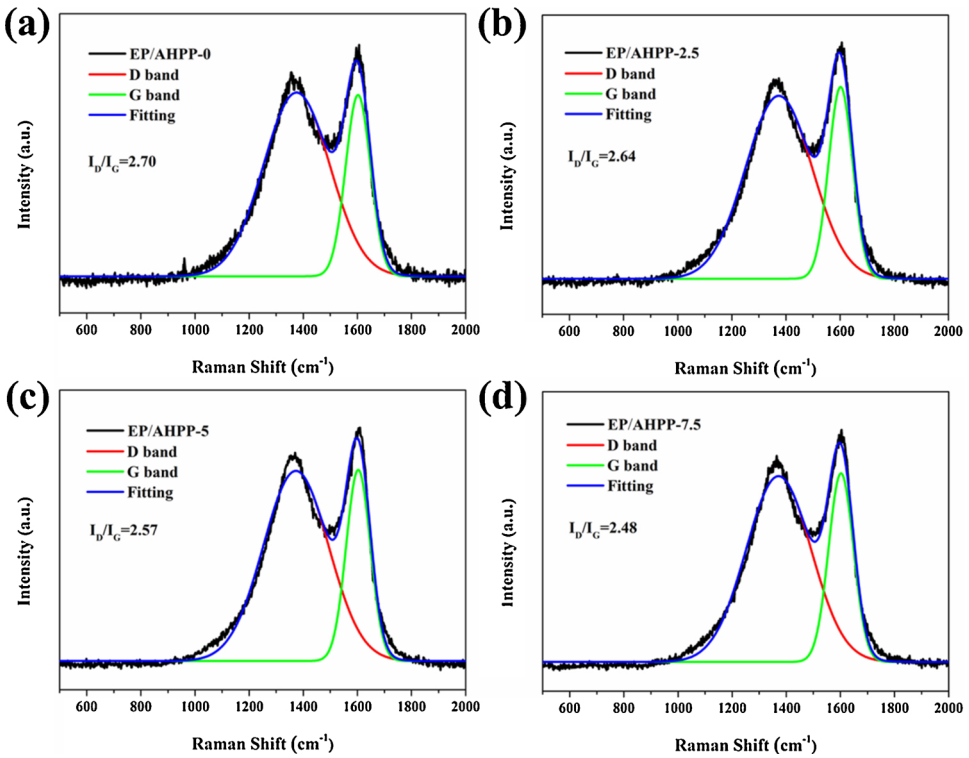

Fig. 11. Raman spectra of the external chars from EP (a), EP/AHPP-2.5 (b), EP/AHPP-5 (c) and EP/AHPP-7.5 (d) after cone calorimeter tests.

they have different absorption intensities. As illustrated in Fig. 9, the intensity of gas emission of EP/AHPP-7.5 composite have markedly reduced, compared to those of the EP, including aromatic compounds, hydrocarbons, which can be aggregated to create smoke particles (Feng et al., 2014; Zhou et al., 2017). Specifically, the signal at 2360 and 2180 cm^{-1} deriving from CO_2 and CO decreases conspicuously during degradation of EP composites, implying the higher char yield and the lower smoke toxicity for EP/AHPP composite. The results of the

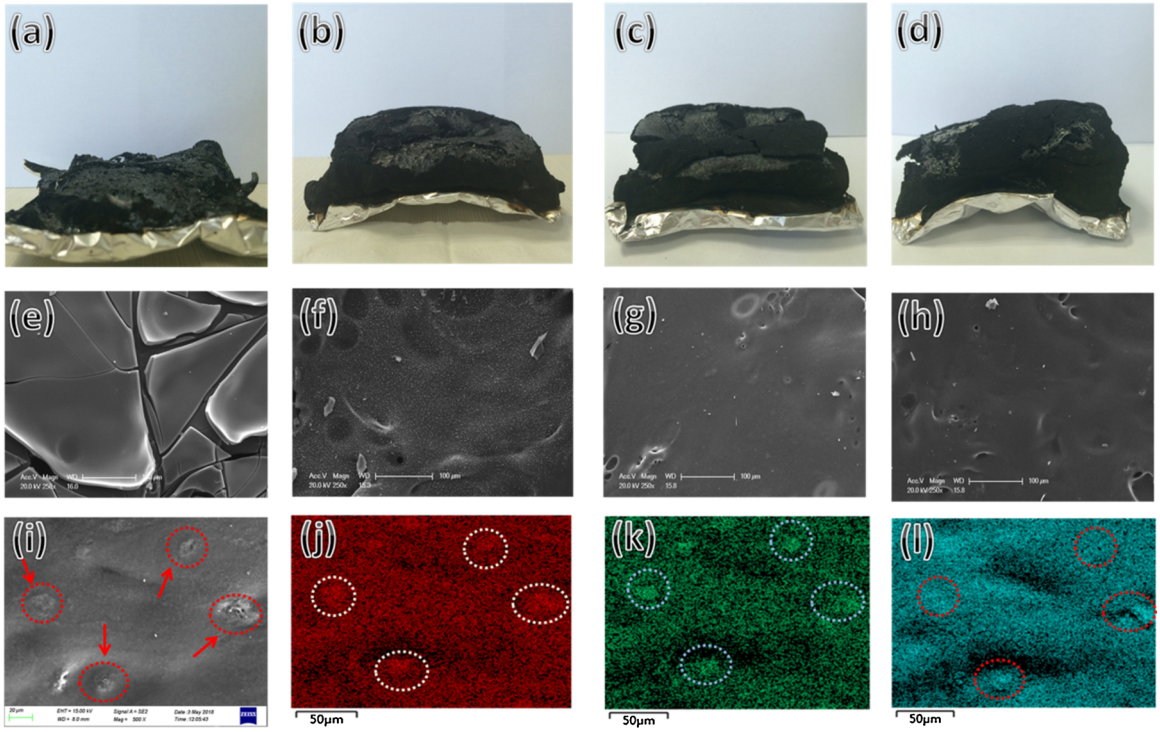

Fig. 10. Photographs (a–d) of the residual char and SEM micrographs (e–h) of surfaces residues of EP, EP/AHPP-2.5, EP/AHPP-5 and EP/AHPP-7.5 after cone calorimeter tests, and elemental distribution from EDX mapping of the EP-AHPP-5 composite (j: P Ka1, k: O Ka1 and l: Al Ka1).

Table 4
Assignments of the peaks in FTIR spectra of EP and EP/AHPP composites.

FTIR (cm^{-1})	Assignments
3412	Stretching vibration of O—H groups
2875–2966	Stretching vibration of $-CH_2$ and $-CH_3$
1090	Stretching vibration of P—O—C
1603	Stretching vibration of C=C_{arom}
1110	O—H bending
1502	fingerprint (C_{arom}—O stretching, $-CH_3$, $-CH_2$- and $-CMe_2$— deformations)
1250	Stretching vibration of P=O
1090	Stretching vibration of O=P—O
820,747	C_{arom}-H bending, rocking

measurement are in good agreement with cone and SSTF analyses, which confirms that the incorporation of AHPP submicro-particles simultaneously decreases both the flame retardance and smoke toxicity suppression for EP composites.

3.5. Analysis of the char residue and potential flame-retardant mechanism

3.5.1. Macroscopic and microscopic morphologies

Basically, the char residues of cured epoxy resin and its composites after ignition can transmit indispensable information associated with the flame-retardant mechanism. Fig. 11a-d present photographs of char residues of EP/AHPP-0, EP/AHPP-2.5, EP/AHPP-5 and EP/AHPP-7.5. It can be depicted that EP burns severely, leaving little, fragmentary and loose char residue that disclosed the underlying foil papers (Fig. 10a). In contrast, EP/AHPP composites present obviously abundant and intumescent char (Fig. 10b–d). The larger volume of residues can afford better shielding action of the underlying material from exposure to heat and oxygen.

The microcosmic views from the EP char residues were further investigated by SEM. As can be seen in Fig. 11a-d, the residue of EP exhibits obvious surface cracks after ignition (Fig. 10a), which cannot act as a shielding effect against heat diffusion. Simultaneously, the heat can easily penetrate through these surface cracks, which is the reason that

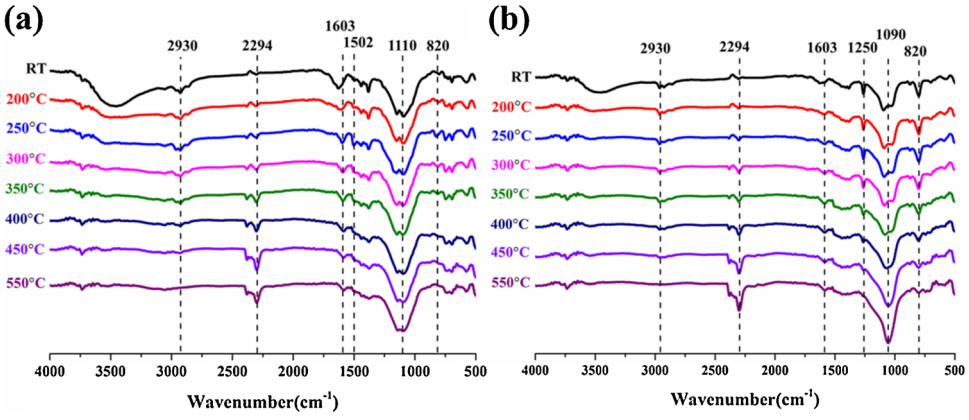

Fig. 12. RT-FTIR spectra of EP (a) and EP/AHPP-7.5 (b) at different pyrolysis temperatures.

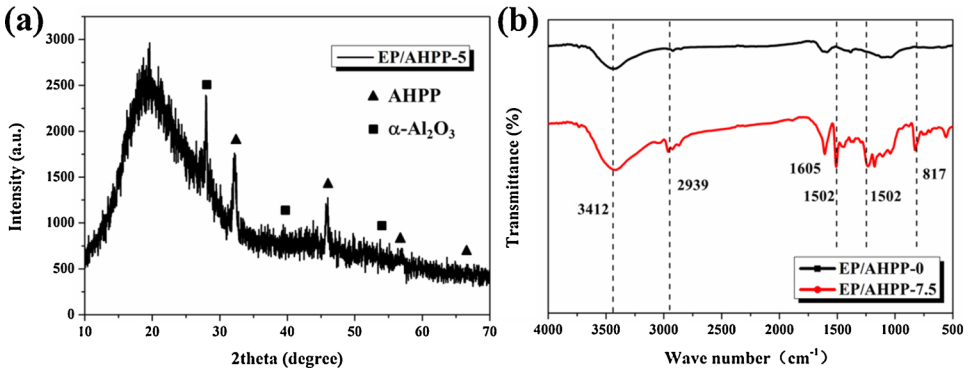

Fig. 13. XRD patterns and FT-IR spectra of the char residue of EP and EP/AHPP-7.5 from cone test.

EP exhibits the lowest LOI value and the highest PHRR and THR. Meanwhile, after AHPP is incorporated, EP composites obtain a much more compact and continuous residues. It is inferred that the dramatically improvement of flame retardance for the EP/AHPP composites, is probably caused by the continuous and compact residues (Wang et al., 2017; Liu et al., 2016b).

3.5.2. Char residue analysis

The graphitic structure of condensed-phased products of EP composites is characterized by Raman spectroscopy (Wawrzyn et al., 2012). Fig. 11 exhibits the Raman spectra of the exterior residues of EP and EP/AHPP composites. The spectra present similar shape including two remarkably overlapping peaks at 1590 and 1360 cm^{-1}. The peak at 1360 cm^{-1} belongs to D band and the peak at 1590 cm^{-1} is named as G band (Fang et al., 2010). Generally, the graphitization degree of the char is estimated by the intensity ratio of the D to G band (I_D/I_G). The I_D/I_G value follows the sequence of EP/AHPP-0 (2.70) > EP/AHPP-2.5 (2.64) > EP/AHPP-5 (2.57) > EP/AHPP-7.5 (2.48), the changes in the Raman ratio is not very large, showing similar graphitization degree. However, Raman spectroscopy analysis and photographs of char residues concluded that the introduction of AHPP is beneficial to producing the compactness of the protective char residues.

3.6. Potential flame retardant mechanism

To further analyse the decomposition behavior, RT-FTIR technique was performed to measure the chemical structural changes in the condensed phase during the thermally oxidative degradation of EP and EP/AHPP-7.5 samples. The residue originated from thermal decomposition under different typical temperatures (R.T., 200 °C, 250 °C, 300 °C, 350 °C, 400 °C, 450 °C and 550 °C) is confirmed by the dynamic FT-IR in the range of 4000-500 cm^{-1}, and the primary bands and peaks of EP and EP/AHPP composites are summarized in Table 4. As portrayed in Fig. 12, the peaks located at 3510, 2930, 2860, 1603, 1502, 1360, 1110, and 820 cm^{-1} belong to EP (Perret et al., 2011). The absorbance of the bands at 2930 and 2860 cm^{-1} is attributed to CH_2 asymmetric and symmetric vibrations and 1502 cm^{-1} corresponding to CH_2 deformation vibration decrease gradually and disappear thoroughly above 550 °C, implying the complete thermal oxidative decomposition of EP main chains (Xiao et al., 2006). As temperatures rise, only the signals at 1603, 1502, 1110, and 820 cm^{-1} are retained, which should be caused by the formation of char residues with multiaromatic structure (Wang et al., 2006b). It is noteworthy that the absorption peaks attributed to the O═P—O— bond, P—O—C and P—O—P vibration at 1250 and 1090 cm^{-1} for EP/AHPP are found in the FT-IR spectra (Liu et al., 2016b; Yuan et al., 2018). However, no obviously changes can be found for the EP, implying that the EP/AHPP composite promotes the formation of the aromatic structure and phosphorous-rich residue during decomposition (Xi et al., 2015). Especially, the absorption at 820 cm^{-1} corresponding to aromatic structure for EP/AHPP composite is remained above 550 °C, implying that the addition of AHPP can enhance the thermo-oxidative stability of the char residue which exhibits a strong barrier action (Liu et al., 2016b).

The char residue of EP and EP composites was further analyzed by XRD and FT-IR. As seen in Fig. 13a, the visible peaks at 31.8°, 45.6°, 56.7° and 66.2° correspond to the diffraction peaks of AHPP, and the others are ascribed well to the Al_2O_3. Accordingly, AHPP submicroparticles thermally degrade to Al_2O_3 (Feng et al., 2017) and cover on the epoxy surfaces. Meanwhile, as exhibited in Fig. 12i-l, the elemental analysis performed by energy dispersive X-ray mappings shows that O, P and Al elements (i.e. the residual char constituents, apart from C) are homogeneously distributed and confirmed the presence of small-scale aggregates. Additionally, from Fig. 13, The FT-IR spectra exhibit a large number of sharp peaks centered at around 1550 to 750 cm^{-1} and can be caused by P—O—C, O═P—O— and P—O—P vibrations (Liu et al., 2016b). Moreover, the peak at 817 cm^{-1} reveals the aromatic structure in the residue of EP-AHPP-7.5 composite, implying that the introduction of AHPP promotes the formation of the aromatic structure and phosphorous-rich residue during decomposition, which is well compatible with the results of RT-FTIR technique.

Based on the results above, the potential flame retardant pathway through charring and intumescence of EP/AHPP binary has been primarily proposed. Firstly, the phosphorus-containing moieties obtained from decomposition of AHPP can catalyze the formation of protective char during degradation of EP, which is beneficial to protecting underlying material from further degradation. By this process, AHPP promotes the formation of char residue with P—O—C and P—O—P moieties, resulting in the formation of the phosphorous-rich residues during thermal degradation. Meanwhile, the much more compact and continuous residues are primarily obtained, as presented in Fig. 10. The char residues act as a useful barrier against the heat and mass transfers thus protect the underlying material from further thermal degradation. According to these facts, the more efficient flame retardance and excellent smoke toxicity suppression performance of EP/AHPP composite exhibits the condensed phase mechanism for its fire resistance.

4. Conclusions

A novel and submicro-scale aluminum branched oligo(phenylphosphonate) (AHPP), successfully synthesized via polycondensation and well characterized, was incorporated into epoxy thermosets in different ratios. The results indicate that the introduction of AHPP submicroparticles can accelerate the thermal degradation of EP composites, which contributed to the formation of compact and protective char residues. The LOI value of EP/AHPP-7.5 was raised to 30.5% from 23.5% for EP and could reach UL-94 V-0 rating. In comparison to pure EP, the cone results displayed that the PHRR and THR values of EP/AHPP-7.5 were decreased by 68.1% and 41.2%, respectively. The higher char yield and larger volume of char residues with stable graphitic structure determined the fire behavior and were beneficial to

improving the flame retardance and smoke toxicity suppression performance of EP composites. Moreover, RT-FTIR analysis exhibited that the char formation containing P—O—P and P—O—C compounds performed a stronger barrier action to protect the EP/AHPP composites. The epoxy resin obtained in this study enabled AHPP to be a potential candidate as a new efficient additive for reducing smoke toxicity of fire safety EP composites, and can be extended to other polymeric material systems

Acknowledgments

The work was financially supported by the National High-tech R&D program (No. 2016YFB0302104), Australian Research Council Discovery Early Career Research Award (No. DE190101176) and National Natural Science Foundation of China (No. 51603200, 51303167).

References

Auvergne, R., Caillol, S., David, G., Boutevin, B., Pascault, J.-P., 2013. Biobased thermosetting epoxy: present and future. Chem. Rev. 114, 1082–1115.
Boogh, L., Pettersson, B., Månson, J.-A.E., 1999. Dendritic hyperbranched polymers as toughenersfor epoxy resins. Polymer 40, 2249–2261.
Braun, U., Balabanovich, A.I., Schartel, B., Knoll, U., Artner, J., Ciesielski, M., Döring, M., Perez, R., Sandler, J.K., Altstädt, V., 2006. Influence of the oxidation state of phosphorus on the decomposition and fire behaviour of flame-retarded epoxy resin composites. Polymer 47, 8495–8508.
Camino, G., Costa, L., Trossarelli, L., 1984. Study of the mechanism of intumescence in fire retardant polymers: part I—thermal degradation of ammonium polyphosphate-pentaerythritol mixtures. Polym. Degrad. Stab. 6, 243–252.
Chen, H.-B., Zhang, Y., Chen, L., Shao, Z.-B., Liu, Y., Wang, Y.-Z., 2010. Novel inherently flame-retardant poly (trimethylene terephthalate) copolyester with the phosphorus-containing linking pendent group. Ind. Eng. Chem. Res. 49, 7052–7059.
Chen, X., Jiao, C., Li, S., Sun, J., 2011. Flame retardant epoxy resins from bisphenol-A epoxy cured with hyperbranched polyphosphate ester. J. Polym. Res 18, 2229–2237.
Choi, J., Kwak, S.-Y., 2007. Hyperbranched poly (ε-caprolactone) as a nonmigrating alternative plasticizer for phthalates in flexible PVC. Environ. Sci. Technol. 41, 3763–3768.
Daasch, L., Smith, D., 1951. Infrared spectra of phosphorus compounds. Anal. Chem. 23, 853–868.
Dogan, M., Unlu, S.M., 2014. Flame retardant effect of boron compounds on red phosphorus containing epoxy resins. Polym. Degrad. Stab. 99, 12–17.
Fang, M., Wang, K., Lu, H., Yang, Y., Nutt, S., 2010. Single-layer graphene nanosheets with controlled grafting of polymer chains. J. Mater. Chem. 20, 1982–1992.
Feng, J., Hao, J., Du, J., Yang, R., 2012. Using TGA/FTIR TGA/MS and cone calorimetry to understand thermal degradation and flame retardancy mechanism of polycarbonate filled with solid bisphenol A bis (diphenyl phosphate) and montmorillonite. Polym. Degrad. Stab. 97, 605–614.
Feng, X., Xing, W., Song, L., Hu, Y., Liew, K.M., 2015. TiO_2 loaded on graphene nanosheet as reinforcer and its effect on the thermal behaviors of poly (vinyl chloride) composites. Chem. Eng. J. 260, 524–531.
Feng, X., Xing, W., Song, L., Hu, Y., 2014. In situ synthesis of a MoS2/CoOOH hybrid by a facile wet chemical method and the catalytic oxidation of CO in epoxy resin during decomposition. J. Mater. Chem. A 2, 13299–13308.
Feng, Y., Hu, J., Xue, Y., He, C., Zhou, X., Xie, X., Ye, Y., Mai, Y.-W., 2017. Simultaneous improvement in the flame resistance and thermal conductivity of epoxy/Al_2O_3 composites by incorporating polymeric flame retardant-functionalized graphene. J. Mater. Chem. A 5, 13544–13556.
Feng, Y., Li, X., Zhao, X., Ye, Y., Zhou, X., Liu, H., Liu, C., Xie, X., 2018a. Synergetic improvement in thermal conductivity and flame retardancy of epoxy/silver nanowires composites by incorporating “Branch-Like” flame-retardant functionalized graphene. ACS Appl. Mater. Interfaces 10, 21628–21641.
Feng, Y., He, C., Wen, Y., Ye, Y., Zhou, X., Xie, X., Mai, Y.-W., 2018b. Superior flame retardancy and smoke suppression of epoxy-based composites with phosphorus/nitrogen co-doped graphene. J. Hazard. Mater. 346, 140–151.
Gu, H., Ma, C., Gu, J., Guo, J., Yan, X., Huang, J., Zhang, Q., Guo, Z., 2016. An overview of multifunctional epoxy nanocomposites. J. Mater. Chem. C 4, 5890–5906.
Horrocks, A.R., Davies, P.J., 2000. Char formation in flame-retarded wool fibres. Part 1. Effect of intumescent on thermogravimetric behaviour. Fire. Mater. 24, 151–157.
Howell, B.A., Oberdorfer, K.L., Ostrander, E.A., 2018. Phosphorus flame retardants for polymeric materials from gallic acid and other naturally occurring multi-hydroxybenzoic acids. Int. J. Polym. Sci. 2018.
Huang, L., Li, Y., Yang, J., Zeng, Z., Chen, Y., 2009. Self-initiated photopolymerization of hyperbranched acrylates. Polymer 50, 4325–4333.
Jeng, R.-J., Shau, S.-M., Lin, J.-J., Su, W.-C., Chiu, Y.-S., 2002. Flame retardant epoxy polymers based on all phosphorus-containing components. Eur. Polym. J. 38, 683–693.
Jian, R., Wang, P., Duan, W., Wang, J., Zheng, X., Weng, J., 2016. Synthesis of a novel P/N/S-containing flame retardant and its application in epoxy resin: thermal property, flame retardance, and pyrolysis behavior. Ind. Eng. Chem. Res. 55, 11520–11527.
Kandola, B.K., Biswas, B., Price, D., Horrocks, A.R., 2010. Studies on the effect of different levels of toughener and flame retardants on thermal stability of epoxy resin. Polym. Degrad. Stab. 95, 144–152.
Li, Z., Wei, P., Yang, Y., Yan, Y., Shi, D., 2014. Synthesis of a hyperbranched poly (phosphamide ester) oligomer and its high-effective flame retardancy and accelerated nucleation effect in polylactide composites. Polym. Degrad. Stab. 110, 104–112.
Li, X., Zhao, Z., Wang, Y., Yan, H., Zhang, X., Xu, B., 2017. Highly efficient flame retardant, flexible, and strong adhesive intumescent coating on polypropylene using hyperbranched polyamide. Chem. Eng. J. 324, 237–250.
Liu, J., Huang, W., Zhou, Y., Yan, D., 2009. Synthesis of hyperbranched polyphosphates by self-condensing ring-opening polymerization of HEEP without catalyst. Macromolecules 42, 4394–4399.
Liu, X., Hao, J., Gaan, S., 2016a. Recent studies on the decomposition and strategies of smoke and toxicity suppression for polyurethane based materials. RSC Adv. 6, 74742–74756.
Liu, C., Chen, T., Yuan, C., Song, C., Chang, Y., Chen, G., Xu, Y., Dai, L., 2016b. Modification of epoxy resin through the self-assembly of a surfactant-like multi-element flame retardant. J. Mater. Chem. A 4, 3462–3470.
Ma, C., Qiu, S., Yu, B., Wang, J., Wang, C., Zeng, W., Hu, Y., 2017. Economical and environment-friendly synthesis of a novel hyperbranched poly (aminomethylphosphine oxide-amine) as co-curing agent for simultaneous improvement of fire safety, glass transition temperature and toughness of epoxy resins. Chem. Eng. J. 322, 618–631.
Mercado, L., Galia, M., Reina, J., 2006. Silicon-containing flame retardant epoxy resins: synthesis, characterization and properties. Polym. Degrad. Stab. 91, 2588–2594.
Perret, B., Schartel, B., Stöß, K., Ciesielski, M., Diederichs, J., Döring, M., Krämer, J., Altstädt, V., 2011. Novel DOPO-based flame retardants in high-performance carbon fibre epoxy composites for aviation. Eur. Polym. J. 47, 1081–1089.
Pinto, U.A., Visconte, L.L.Y., Nunes, R.C.R., 2001. Mechanical properties of thermoplastic polyurethane elastomers with mica and aluminum trihydrate. Eur. Polym. J. 37, 1935–1937.
Ren, H., Sun, J., Wu, B., Zhou, Q., 2007. Synthesis and properties of a phosphorus-containing flame retardant epoxy resin based on bis-phenoxy (3-hydroxy) phenyl phosphine oxide. Polym. Degrad. Stab. 92, 956–961.
Shi, Y., Yu, B., Zheng, Y., Yang, J., Duan, Z., Hu, Y., 2018. Design of reduced graphene oxide decorated with DOPO-phosphanomidate for enhanced fire safety of epoxy resin. J. Colloid Interface Sci. 521, 160–171.
Shi, Y., Liu, C., Liu, L., Fu, L., Yu, B., Lv, Y., Yang, F., Song, P., 2019. Strengthening, toughing and thermally stable ultra-thin MXene nanosheets/polypropylene nanocomposites via nanoconfinement. Chem. Eng. J., 122267.
Shieh, J.-Y., Wang, C.-S., 2001. Synthesis of novel flame retardant epoxy hardeners and properties of cured products. Polymer 42, 7617–7625.
Täuber, K., Marsico, F., Wurm, F.R., Schartel, B., 2014. Hyperbranched poly (phosphoester) s as flame retardants for technical and high performance polymers. Polym. Chem. 5, 7042–7053.
Wan, J., Li, C., Bu, Z.-Y., Xu, C.-J., Li, B.-G., Fan, H., 2012. A comparative study of epoxy resin cured with a linear diamine and a branched polyamine. Chem. Eng. J. 188, 160–172.
Wan, J., Gan, B., Li, C., Molina-Aldareguia, J., Li, Z., Wang, X., Wang, D.-Y., 2015. A novel biobased epoxy resin with high mechanical stiffness and low flammability: synthesis, characterization and properties. J. Mater. Chem. A 3, 21907–21921.
Wang, Q., Shi, W., 2006a. Synthesis and thermal decomposition of a novel hyperbranched polyphosphate ester used for flame retardant systems. Polym. Degrad. Stab. 91, 1289–1294.
Wang, Q., Shi, W., 2006b. Photopolymerization and thermal behaviors of acrylated benzenephosphonates/epoxy acrylate as flame retardant resins. Eur. Polym. J. 42, 2261–2269.
Wang, X., Song, L., Xing, W., Lu, H., Hu, Y., 2011. A effective flame retardant for epoxy resins based on poly (DOPO substituted dihydroxyl phenyl pentaerythritol diphosphonate). Mater. Chem. Phys. 125, 536–541.
Wang, X., Zhou, S., Guo, W.-W., Wang, P.-L., Xing, W., Song, L., Hu, Y., 2017. Renewable cardanol-based phosphate as a flame retardant toughening agent for epoxy resins. ACS Sustainable Chem. Eng. 5, 3409–3416.
Wang, X., Zhou, S., Xing, W., Yu, B., Feng, X., Song, L., Hu, Y., 2013. Self-assembly of Ni–Fe layered double hydroxide/graphene hybrids for reducing fire hazard in epoxy composites. J. Mater. Chem. A 1, 4383–4390.
Wang, D., Zheng, Z., Hong, C., Liu, Y., Pan, C., 2006a. Michael addition polymerizations of difunctional amines (AA′) and triacrylamides (B3). J. Polym. Sci., Part A: Polym. Chem. 44, 6226–6242.
Wang, G.-A., Cheng, W.-M., Tu, Y.-L., Wang, C.-C., Chen, C.-Y., 2006b. Characterizations of a new flame-retardant polymer. Polym. Degrad. Stab. 91, 3344–3353.
Wawrzyn, E., Schartel, B., Ciesielski, M., Kretzschmar, B., Braun, U., Döring, M., 2012. Are novel aryl phosphates competitors for bisphenol A bis (diphenyl phosphate) in halogen-free flame-retarded polycarbonate/acrylonitrile–butadiene–styrene blends? Eur. Polym. J. 48, 1561–1574.
Wu, K., Song, L., Hu, Y., Lu, H., Kandola, B.K., Kandare, E., 2009. Synthesis and characterization of a functional polyhedral oligomeric silsesquioxane and its flame retardancy in epoxy resin. Prog. Org. Coat. 65, 490–497.
Xi, W., Qian, L., Chen, Y., Wang, J., Liu, X., 2015. Addition flame-retardant behaviors of expandable graphite and [bis (2-hydroxyethyl) amino]-methyl-phosphonic acid dimethyl ester in rigid polyurethane foams. Polym. Degrad. Stab. 122, 36–43.
Xiao, J., Hu, Y., Yang, L., Cai, Y., Song, L., Chen, Z., Fan, W., 2006. Fire retardant synergism between melamine and triphenyl phosphate in poly (butylene terephthalate). Polym. Degrad. Stab. 91, 2093–2100.
Xie, J., Hu, L., Shi, W., Deng, X., Cao, Z., Shen, Q., 2008. Synthesis and characterization of hyperbranched polytriazole via an ‘A2 + B3′approach based on click chemistry.

Polym. Int. 57, 965–974.
Xu, Y.-J., Wang, J., Tan, Y., Qi, M., Chen, L., Wang, Y.-Z., 2018. A novel and feasible approach for one-pack flame-retardant epoxy resin with long pot life and fast curing. Chem. Eng. J. 337, 30–39.
Xu, W., Wirasaputra, A., Liu, S., Yuan, Y., Zhao, J., 2015. Highly effective flame retarded epoxy resin cured by DOPO-based co-curing agent. Polym. Degrad. Stab. 122, 44–51.
You, G., Cheng, Z., Tang, Y., He, H., 2015. Functional group effect on char formation, flame retardancy and mechanical properties of phosphonate–triazine-based compound as flame retardant in epoxy resin. Ind. Eng. Chem. Res. 54, 7309–7319.
Yu, B., Xing, W., Guo, W., Qiu, S., Wang, X., Lo, S., Hu, Y., 2016. Thermal exfoliation of hexagonal boron nitride for effective enhancements on thermal stability, flame retardancy and smoke suppression of epoxy resin nanocomposites via sol–gel process. J. Mater. Chem. A 4, 7330–7340.
Yuan, Y., Yang, H., Yu, B., Shi, Y., Wang, W., Song, L., Hu, Y., Zhang, Y., 2016. Phosphorus and nitrogen-containing polyols: synergistic effect on the thermal property and flame retardancy of rigid polyurethane foam composites. Ind. Eng. Chem. Res. 55, 10813–10822.
Yuan, Y., Wang, W., Shi, Y., Song, L., Ma, C., Hu, Y., 2019. The influence of highly dispersed Cu_2O-anchored MoS_2 hybrids on reducing smoke toxicity and fire hazards for rigid polyurethane foam. J. Hazard. Mater., 121028.
Yuan, Y., Ma, C., Shi, Y., Song, L., Hu, Y., Hu, W., 2018. Highly-efficient reinforcement and flame retardancy of rigid polyurethane foam with phosphorus-containing additive and nitrogen-containing compound. Mater. Chem. Phys. 211, 42–53.
Zang, L., Wagner, S., Ciesielski, M., Müller, P., Döring, M., 2011. Novel star-shaped and hyperbranched phosphorus-containing flame retardants in epoxy resins. Polym. Adv. Technol. 22, 1182–1191.
Zhang, Y., Yu, B., Wang, B., Liew, K.M., Song, L., Wang, C., Hu, Y., 2017. Highly effective P–P synergy of a novel DOPO-based flame retardant for epoxy resin. Ind. Eng. Chem. Res. 56, 1245–1255.
Zhou, K., Tang, G., Gao, R., Jiang, S., 2018. In situ growth of 0D silica nanospheres on 2D molybdenum disulfide nanosheets: towards reducing fire hazards of epoxy resin. J. Hazard. Mater. 344, 1078–1089.
Zhou, K., Gao, R., Qian, X., 2017. Self-assembly of exfoliated molybdenum disulfide (MoS_2) nanosheets and layered double hydroxide (LDH): towards reducing fire hazards of epoxy. J. Hazard. Mater. 338, 343–355.